Relative time seislet transform

Zhicheng Geng[1], Xinming Wu[1], Sergey Fomel[1], and Yangkang Chen[2]

ABSTRACT

The seislet transform uses the wavelet-lifting scheme and local slopes to analyze the seismic data. In its definition, the designing of prediction operators specifically for seismic images and data is an important issue. We have developed a new formulation of the seislet transform based on the relative time (RT) attribute. This method uses the RT volume to construct multiscale prediction operators. With the new prediction operators, the seislet transform gets accelerated because distant traces get predicted directly. We apply our method to synthetic and real data to demonstrate that the new approach reduces computational cost and obtains excellent sparse representation on test data sets.

INTRODUCTION

Sparse transforms aim to represent the most important information of an image with few coefficients in the transform domain while obtaining a good-quality approximation of the original image. Over the past several decades, different types of wavelet-like transforms have been proposed and successfully applied in image compression and denoising (Hennenfent and Herrmann, 2006; Li and Gao, 2013), such as curvelets (Starck et al., 2002; Ma and Plonka, 2010), contourlets (Do and Vetterli, 2005), shearlets (Labate et al., 2005), directionlets (Velisavljevic et al., 2006), and bandelets (Le Pennec and Mallat, 2005). The strong anisotropic selectivity of these wavelet-like transforms helps achieve excellent data compression and accurate reconstruction for seismic images.

Fomel and Liu (2010) introduce the seislet transform, which is a digital wavelet-like transform designed specifically for seismic data. Based on the lifting scheme used in digital wavelet transform construction (Sweldens, 1995), the seislet transform follows dominant local slopes obtained by plane-wave destruction (PWD) (Fomel, 2002) to predict seismic events. Instead of using PWD, Liu and Fomel (2010) use offset continuation (OC) to construct updating and prediction operators. The OC-seislet transform has better performance than the PWD-seislet transform in characterizing and compressing structurally complex prestack reflection data. To reduce sensitivity to strong noise interference, Liu et al. (2015) propose a velocity-dependent seislet transform. In this method, the normal moveout equation was introduced to serve as a connection between the local slope and scanned velocities. Chen and Fomel (2018) use empirical-mode decomposition (EMD) to obtain smoothly nonstationary data and then apply the 1D nonstationary seislet transform to the data. This new approach was called the EMD-seislet transform, and it has shown excellent performance in attenuating random noise. Several recent studies show the superiority of the seislet transform on sparse representation of seismic data over the Fourier transform, the wavelet transform, and the curvelet transform (Fomel and Liu, 2010; Gan et al., 2015; Chen and Fomel, 2018).

With the ability to compress and reconstruct seismic images, the seislet transform has been successfully applied in seismic data processing such as noise attenuation (Chen, 2016; Chen et al., 2016), deblending (Chen et al., 2014; Gan et al., 2016), and data interpolation (Liu et al., 2013; Gan et al., 2016), However, the original implementation of PWD-seislet transform requires recursively computation when predicting distant traces, which increases its computation cost, especially when the data set is very large. In addition, the smooth slopes from PWD in the original seislet transform can fail to correctly follow reflections across discontinuities including faults and unconformities. Therefore, geologically meaningful discontinuities may not be optimally compressed.

The relative time (RT) volume $\tau(x, y, t)$ has different meanings in different domains. In the seismic image domain, the RT is the same as the relative geologic time (Stark, 2003, 2004) and each RT contour corresponds to a geologic horizon. However, RT volumes of seismic gathers do not necessarily have geologic meaning because, in this case, constant RT contours align with seismic events. There are several ways to generate an RT volume. One can always pick out

as many horizons or events as possible to obtain it, which is simple but laborious. The RT volume can also be generated by unwrapping the seismic instantaneous phase (Stark, 2003; Wu and Zhong, 2012). Fomel (2010) uses local slopes of seismic events estimated by PWD (Fomel, 2002) to generate the RT volume, which has superior computational performance. The RT volume already has been successfully applied in missing well-log data prediction (Bader et al., 2018) and seismic horizon construction (Wu and Hale, 2015).

In this paper, we propose a new implementation of the seislet transform, called the RT-seislet transform, by using the RT obtained from the predictive painting (Fomel, 2010) to construct prediction operators for the seislet transform. In this way, prediction of one trace from distant traces is computed directly and accurately, which saves a lot of computation and has better performance with faults and unconformities. By applying the new formulation of the seislet transform to synthetic and real data, we demonstrate that the proposed method is efficient and able to preserve discontinuities, while achieving excellent sparse representation of seismic data.

This paper is organized as follows: We first review the seislet transform and the estimation of an RT volume. Then, we incorporate RT attribute to construct new formulation of prediction and update operators for the seislet transform. Finally, we test the proposed RT-seislet transform on synthetic and real data sets and compare its performance with the PWD-seislet transform.

THEORY

Reviews of the 2D seislet transform

As proposed by Fomel and Liu (2010), the seislet transform can be constructed using the lifting scheme (Sweldens, 1995). The procedure of the lifting scheme is as follows:

1) Arrange the input data as a sequence of records. In the seislet transform, the input data are common-shot gather or seismic image.
2) Divide the arranged records into even and odd components **e** and **o**. For the 2D seislet transform, each trace is a component and the seismic data are split into two parts according to the trace indices.
3) Find the residual **r** between the odd component and its prediction from the even component

$$\mathbf{r} = \mathbf{o} - \mathbf{P}[\mathbf{e}], \qquad (1)$$

where **P** is a *prediction* operator.
4) Using the difference from the previous step to get a coarse approximation **c** of the data by updating the even component

$$\mathbf{c} = \mathbf{e} + \mathbf{U}[\mathbf{r}], \qquad (2)$$

where **U** is an *update* operator.
5) The coarse approximation **c** obtained from last step becomes the new data, and previous steps are applied to the new data at the next scale level.

The coarse approximation **c** from the final scale and the residual difference **r** from all scales form the result of the seislet transform.

The prediction and update operators are defined, for example, by modifying operators in the construction of Cohen–Daubechies–Feauveau 5/3 biorthogonal wavelets (Cohen et al., 1992) as follows:

$$\mathbf{P}[\mathbf{e}]_k = (\mathbf{S}_k^{(+)}[\mathbf{e}_{k-1}] + \mathbf{S}_k^{(-)}[\mathbf{e}_k])/2 \qquad (3)$$

and

$$\mathbf{U}[\mathbf{r}]_k = (\mathbf{S}_k^{(+)}[\mathbf{r}_{k-1}] + \mathbf{S}_k^{(-)}[\mathbf{r}_k])/4, \qquad (4)$$

where $\mathbf{S}_k^{(+)}$ and $\mathbf{S}_k^{(-)}$ can accomplish the prediction of a trace from its left and right neighbors, respectively. The predictions need to be applied at different scales. For the 2D seislet transform, different scales mean different distances between traces. More accurate higher order formulations are possible. Following the inverse lifting scheme from coarse to fine scale, the inverse seislet transform can be constructed.

RT volume estimation

In the proposed method, predictive painting (Fomel, 2010), based on the prediction operator arising from PWD (Fomel, 2002), is used to generate the RT volume. In the predictive painting, after local slopes are estimated, an RT volume is computed by spreading time values of reference traces along dominant event slopes throughout the whole seismic volume.

Using linear operator notation, PWD operation is defined as

$$\mathbf{d} = \mathbf{D}\mathbf{s}, \qquad (5)$$

where $\mathbf{s} = \begin{bmatrix} \mathbf{s}_1 & \mathbf{s}_2 & \cdots & \mathbf{s}_N \end{bmatrix}^T$ is a collection of seismic traces and **d** denotes the residual from destruction. The term **D** is the destruction operator defined as

$$\mathbf{D} = \begin{bmatrix} \mathbf{I} & 0 & 0 & \cdots & 0 \\ -\mathbf{P}_{1,2} & \mathbf{I} & 0 & \cdots & 0 \\ 0 & -\mathbf{P}_{2,3} & \mathbf{I} & \cdots & 0 \\ \vdots & \ddots & \ddots & \ddots & \vdots \\ 0 & \cdots & 0 & -\mathbf{P}_{N-1,N} & \mathbf{I} \end{bmatrix}, \qquad (6)$$

where **I** denotes the identity matrix and $\mathbf{P}_{i,i+1}$ is an operator that predicts the $(i+1)$th trace from the ith trace according to the local slope of the seismic event or seismic horizon.
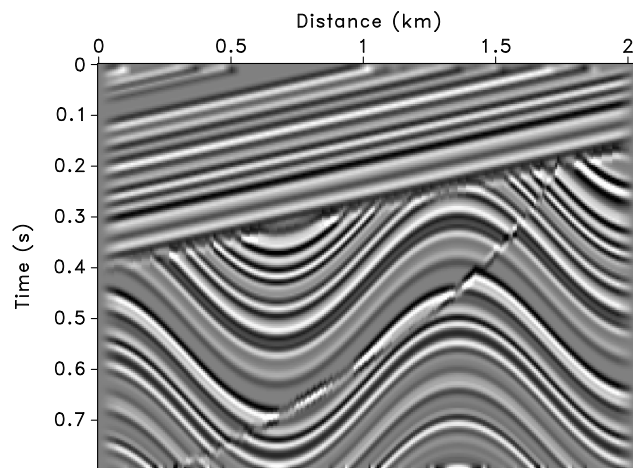

Figure 1. Synthetic seismic image from Claerbout (2000).

By a simple recursion, a trace can be predicted using a distant trace. For example, $\mathbf{P}_{r,k}$, predicting the kth trace from the rth trace, is defined as

$$\mathbf{P}_{r,k} = \mathbf{P}_{k-1,k}\mathbf{P}_{k-2,k-1} \cdots \mathbf{P}_{r+1,r+2}\mathbf{P}_{r,r+1}. \qquad (7)$$
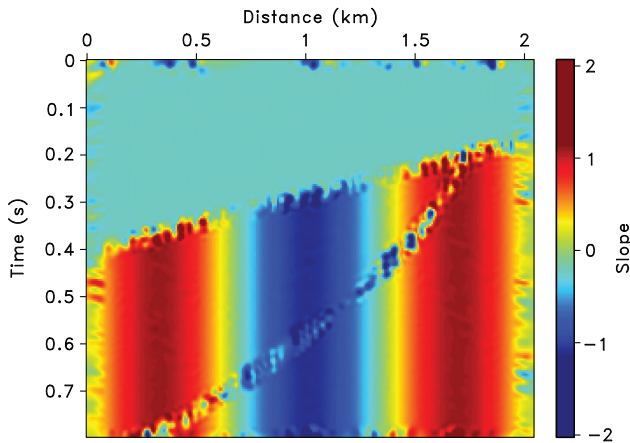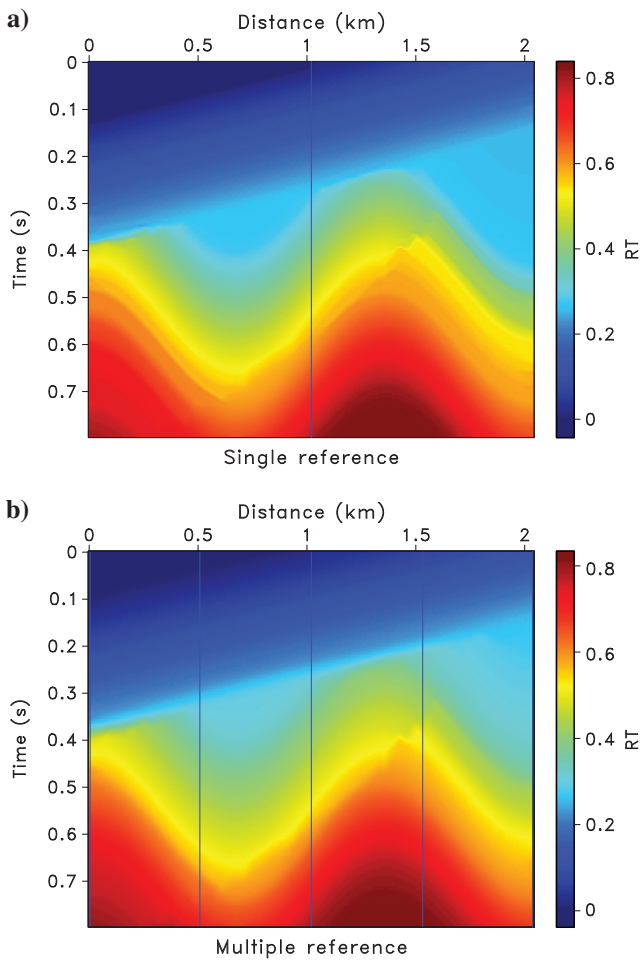

Figure 2. Local slopes estimated from Figure 1.

a)

Single reference

b)

Multiple reference

Figure 3. The RT estimated by predictive painting from Figure 1 using (a) a single reference trace and (b) multiple reference traces.

Then, the prediction of trace $\mathbf{s}_r$, given a reference trace $\mathbf{s}_r$ is accomplished by

$$\mathbf{s}_k^{\text{pre}} = \mathbf{P}_{r,k}\mathbf{s}_r. \qquad (8)$$

After determining the prediction operators in equation 6 by PWD, the predictive painting algorithm recursively spreads information from a reference trace to the whole seismic data volume by following local slopes using equation 8. If the information spread by the predictive painting is the time coordinates, an RT volume is easily computed.

Figure 1 shows a synthetic image with several complex geologic structures. Local slopes corresponding to Figure 1 are shown in Figure 2, which are estimated by PWD. Figure 3a shows the RT volume calculated by the predictive painting using local slopes in Figure 2. The reference trace of this RT volume is in the center of the image, which is marked as a vertical line in Figure 3a. This single reference RT volume is used to flatten the input seismic image (Figure 1) by unshifting each trace using the information it contains because RT indicates how much a given trace is shifted with respect to the reference trace. The flattened image is shown in Figure 4a. Another RT volume with multiple references, shown in Figure 3b, is generated by selecting five reference traces and calculating the average of all
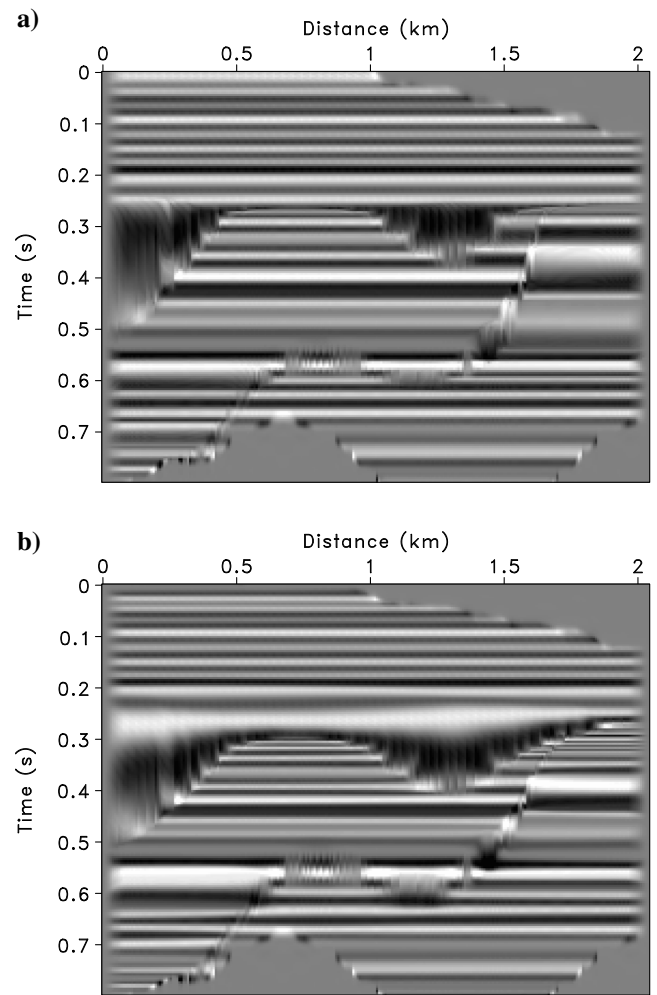

a)

b)

Figure 4. Flattened images using RT volumes from (a) Figure 3a and (b) Figure 3b.
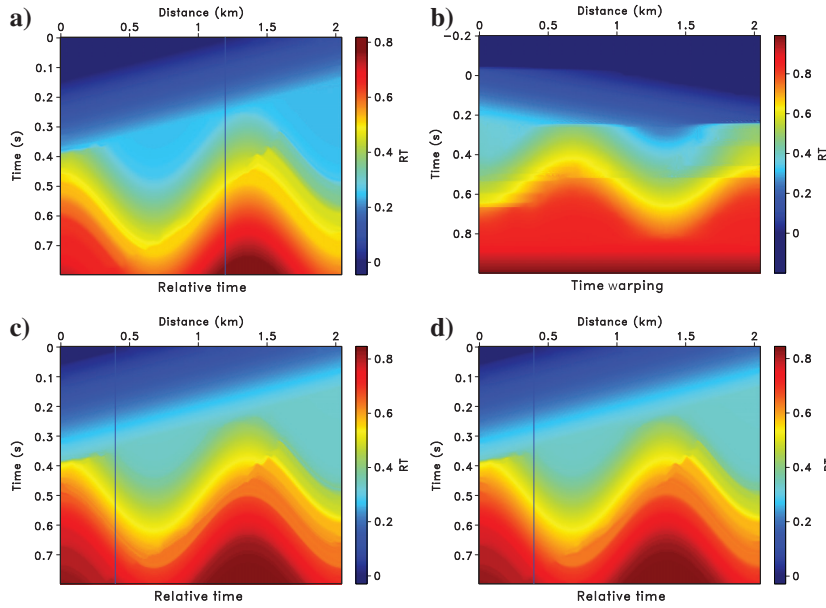
Figure 5. (a) The RT volume obtained by the predictive painting and the reference trace is the 150th trace. (b) Time warping of (a). (c) RT volume obtained by equation 10. (d) The RT volume obtained by the predictive painting and the reference trace is the 50th trace.
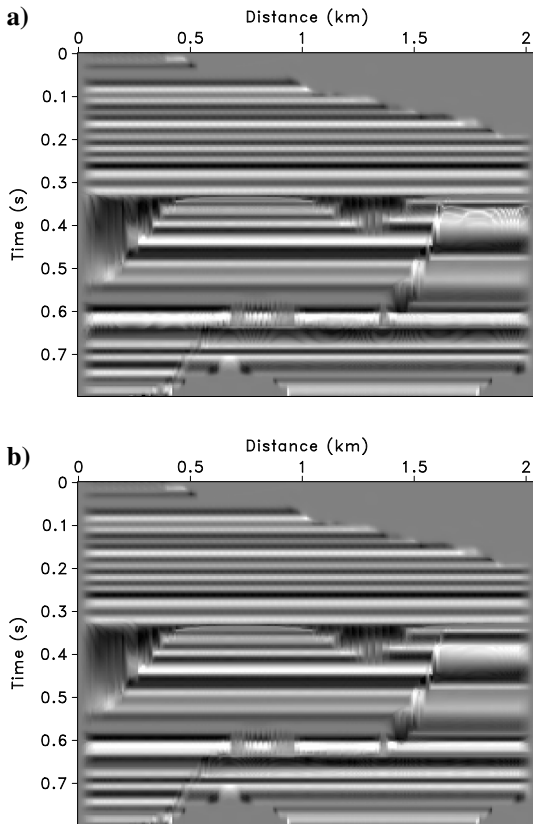

Figure 6. Flattened images using RT volumes from (a) Figure 5c and (b) Figure 5d.

the estimated RT volumes. Figure 4b shows the corresponding flattened image. The comparison between two flattened seismic images (Figure 4a and 4b) indicates that the RT volume with only one reference trace does not necessarily have information about all seismic events because there are discontinuities such as faults and unconformities, whereas the RT volume computed with more reference traces contains more information.

RT formulation of prediction and update operators

RT contains the relationship between traces. From RT volume, it is straightforward to obtain the shift of one trace with respect to the reference. Therefore, the trace prediction using RT volumes is formulated as follows:

$$\mathbf{s}_k^{\text{pre}}(t) = \mathbf{s}_r(\tau_{k,r}(t)), \tag{9}$$

where $\mathbf{s}_k$ and $\mathbf{s}_r$ denote the kth and the rth trace, respectively, and $\tau_{k,r}(t)$ is the RT value of the kth trace with the rth trace as the reference trace, indicating the shift of the kth trace with respect to the rth trace. According to equation 9, the prediction of the kth trace from the rth trace is easily accomplished by applying forward interpolation to the rth trace using corresponding RT values. In the proposed method, we use equation 9 to define operators $\mathbf{S}$ in equations 3 and 4 to construct corresponding prediction and update operators. In this way, a trace is predicted from a distant trace directly by the RT attribute instead of the recursive computation used in the PWD-seislet transform. In addition, because an accurate RT volume stores information about all horizons and structural discontinuities including faults and unconformities, predictions of traces around discontinuities using equation 9 are accurate. Therefore, a better delineation of faults and unconformities can be achieved.

In computing an RT volume, we need to first choose one or multiple reference traces. After computing the RT volume, the RT attribute between any two traces is easily obtained from one RT volume using

$$\tau_{k,r}(t) = \tau_{r,l}^{-1}(\tau_{k,l}(t)), \tag{10}$$

where $\tau_{j,i}(t)$ represents the RT value of the jth trace with the ith trace as the reference trace and $\tau_{r,l}^{-1}(t)$ is the time warping (Burnett and Fomel, 2009) of $\tau_{r,l}(t)$. According to equation 10, given the shift information $\tau_{r,l}(t)$ and $\tau_{k,l}(t)$, the shift relationship between the kth trace and the rth trace can be obtained by applying an inverse interpolation to $\tau_{r,l}(t)$ using $\tau_{k,l}(t)$. Then, equation 9 is applied to implement the prediction of the kth trace from the rth trace. Therefore, only one RT volume is needed for the proposed implementation of the seislet transform.

Figure 5 shows an example of implementing equation 10 to compute an RT volume from another one with different reference traces. The RT volume in Figure 5a is obtained by the predictive painting with the 150th trace as the reference trace. This RT volume can be represented by $\tau_{k,150}(t), k = 1, 2, \ldots, n$. Figure 5b shows the time warping of this RT volume. We extract the 50th trace from Figure 5b, which is denoted by $\tau_{50,150}^{-1}(t)$. Then, by implementing

equation 10, i.e., inverse interpolating $\tau_{50,150}^{-1}(t)$ using the whole RT volume ($\tau_{k,150}(t)$, $k = 1, 2, \ldots, n$), we can get a new RT volume, as shown in Figure 5c ($\tau_{k,50}(t)$, $k = 1, 2, \ldots, n$). Here, we use the 50th trace as the reference trace. To evaluate the effectiveness of equation 10, RT volumes from Figure 5c and 5d are used to flatten Figure 1. Flattened images are shown in Figure 6. Small differences between Figure 6a and 6b indicate that these two RT volumes (Figure 5c and 5d) contain similar information, which demonstrates that equation 10 can be used to obtain the relationship between any two traces from a single RT volume.

Workflow

The workflow of the proposed method is shown in Figure 7. As we can see, the proposed approach is convenient to implement because only one RT volume is needed before applying the new formulation of the seislet transform. In the proposed approach, we need to first use PWD to compute the local slopes of the input seismic data such that the RT volume can be computed by the predictive painting from the estimated slopes, as discussed in the previous section. With the help of the generated RT volume, the RT-seislet transform is then applied to the input data to get coefficients in the RT-seislet transform domain. With the transformed data, signal processing tasks, such as data reconstruction and noise attenuation, can be easily applied.
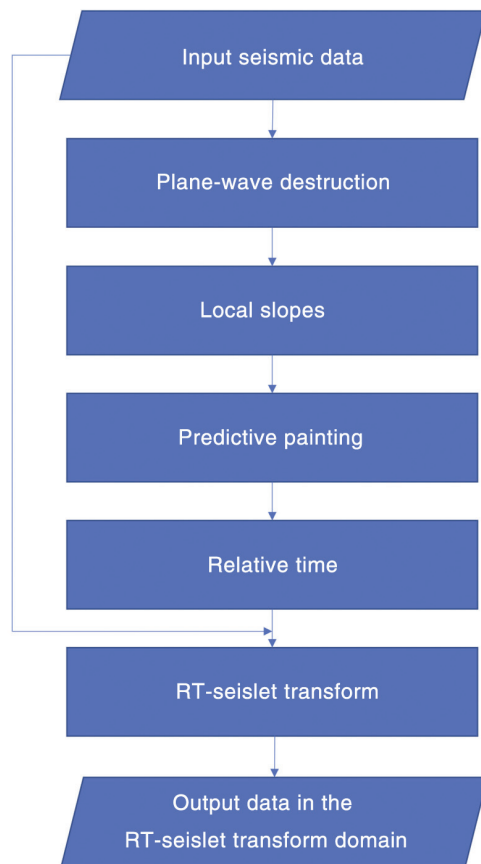

Figure 7. Workflow of the proposed RT-seislet transform.

SYNTHETIC DATA EXAMPLE

We use the same data example from Figure 1 to demonstrate the performance of the proposed method in efficient data reconstruction. Figure 8 shows the RT calculated from the image using the
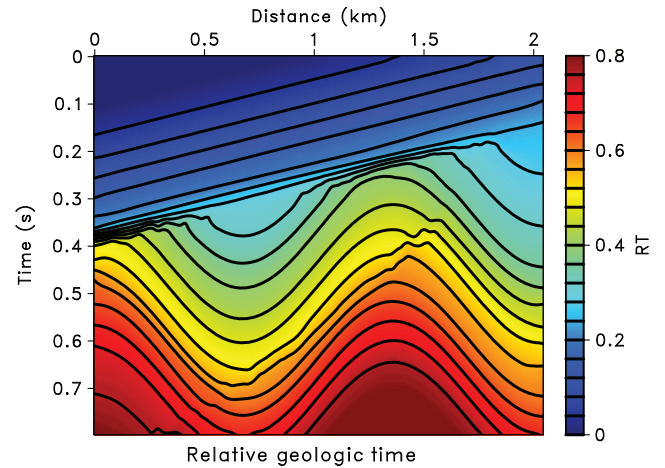

Figure 8. The RT volume estimated by the predictive painting using multiple reference traces.
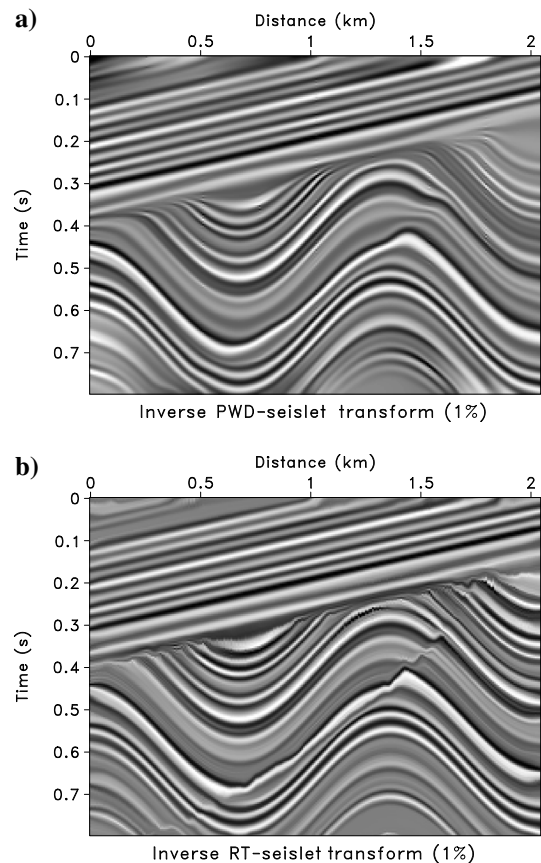

Figure 9. Synthetic seismic image reconstruction by thresholding coefficients and keeping only 1% of significant coefficients using the (a) inverse PWD-seislet transform and (b) inverse RT-seislet transform.

predictive painting with multiple reference traces. We applied the original PWD-seislet transform and the RT-seislet transform to this image. Then, we threshold the coefficients and keep only the largest ones from both transforms to reconstruct the same original data. By using the same percent (1%) of large coefficients, the reconstruction from the new formulation (Figure 9b) recovers more accurate amplitude values and better preserves structural discontinuities near faults and unconformities than the one from the PWD-seislet transform (Figure 9a).

A comparison between coefficients from the PWD-seislet transform and the RT-seislet transform is shown in Figure 10. The minor difference of their decay rate indicates that the PWD-seislet transform and the proposed transform obtain the same sparsity for the input data. Figure 11 shows the plot of central processing unit time against the number of traces. The proposed formulation of the seislet transform shows promising computation efficiency because the prediction of a trace using distant traces is accomplished directly instead of recursively as in the original PWD-seislet transform.
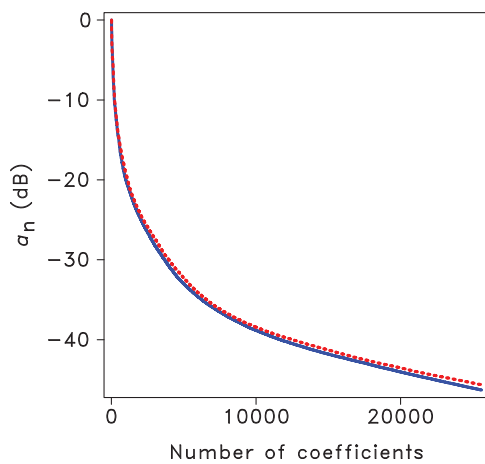

Figure 10. Normalized coefficients from the PWD-seislet transform (the dashed red line) and the RT-seislet transform (the solid blue line) sorted from large to small on a decibel scale.
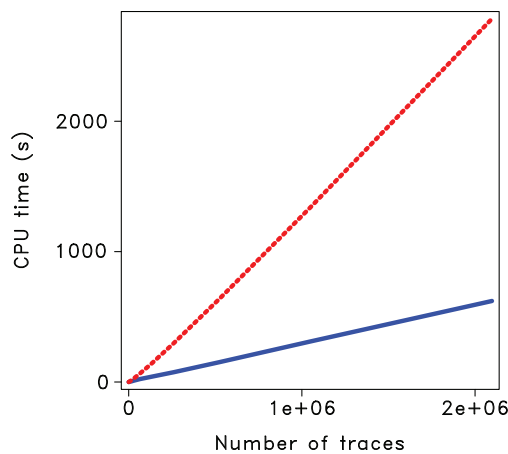

Figure 11. The CPU time of the PWD-seislet transform (the dashed red line) and the RT-seislet transform (the solid blue line) versus the number of traces.

For the purpose of testing the sensitivity of the RT-seislet transform to noise, we add random noise to the synthetic model and use the signal-to-noise ratio (S/N) as the measurement:

$$S/N = 10 \log_{10} \frac{\|s_{true}\|_2^2}{\|s_{true} - s\|_2^2}, \tag{11}$$
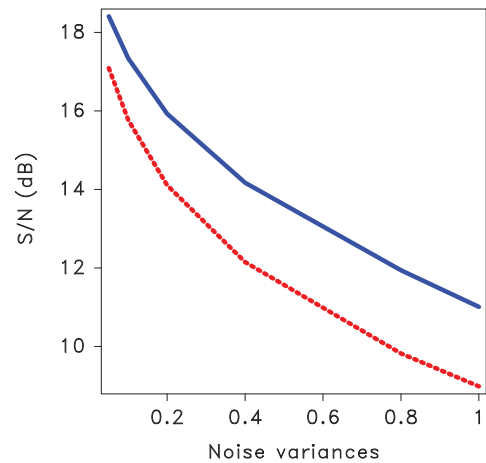

Figure 12. The S/N diagram of the PWD-seislet transform (the dashed red line) and the RT-seislet transform (the solid blue line) with respect to the noise level (variance value).
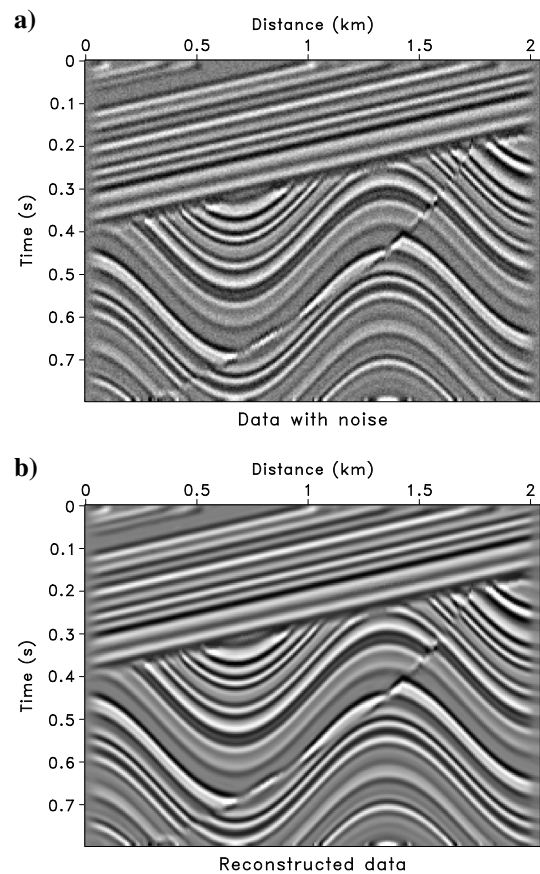

Figure 13. (a) Noisy data and (b) reconstructed data using 10% coefficients (S/N = 17.19).

where $\mathbf{s}_{\text{true}}$ is the original data and $\mathbf{s}$ denotes the reconstructed data (Figure 9b) or noisy data. We plot the S/Ns of reconstructed data using the inverse PWD-seislet transform and the inverse RT-seislet transform with respect to the noise variance in Figure 12. Apparently, as the noise level increases, the performance of the RT-seislet gets worse, which shows that the proposed method is sensitive to noise. But, compared with the original PWD-seislet transform, the new method has superior performance that is less sensitive to noise. Figure 13 shows one example of the noisy data and the reconstructed data. The S/N of Figure 13b is 17.19 dB.

Figure 14 presents another synthetic example. Figure 14a shows the synthetic shot gather with three hyperbolic events, and Figure 14b shows the data reconstruction by the RT-seislet transform using only 1% of the most significant coefficients. We use the first, middle, and last traces as the reference traces to compute the RT volume. The residual between the synthetic shot gather and the reconstruction result is shown in Figure 14c. For this simple synthetic shot gather, the proposed method achieves an excellent data reconstruction result.

2D FIELD DATA EXAMPLE

To further test the proposed method, we use a common-midpoint gather from the North Sea data set (Figure 15). Figure 16a shows the data in the seislet transform domain. We observe that significant coefficients are apparent in only a narrow area on the left, which indicates the excellent compression ability of the proposed RT formulation of the seislet transform. The field data reconstruction using only 1% of the most significant RT-seislet coefficients is shown in Figure 16b. The reconstructed image retains the most important seismic events in the original seismic data.

If we mute the RT-seislet coefficients at fine scales while keeping the significant coefficients at coarse scales (Figure 17b), the inverse RT-seislet transform enables effective denoising, removing incoherent noise from the gather. The result of denoising is shown in Figure 17c. Figure 17d shows the removed noise section using the proposed implementation of the seislet transform.

The RT seislet is also able to perform interpolation. We add two more scales with small random noise to Figure 16a and interpolate the RT volume by a factor of four. Then, the interpolated shot gather is obtained and the number of traces is increased by four. The extended data in the seislet transform domain are shown in Figure 18a.

Figure 18b shows the interpolated shot gather. Figure 19 shows the f-k spectrum of the zero-padded field data and the interpolated gather. The zero-padded shot gather is generated by manually padding zero traces between two traces. In this example, the seislet transform domain is extended with random noise because there is unpredictable noise in the real case.

3D FIELD DATA EXAMPLE

We also test the proposed method on a 3D data set. Figure 20a shows the Teapot Dome seismic data set. After the inline and cross-line slopes (Figure 21) are estimated, the RT volume (Figure 20b) is
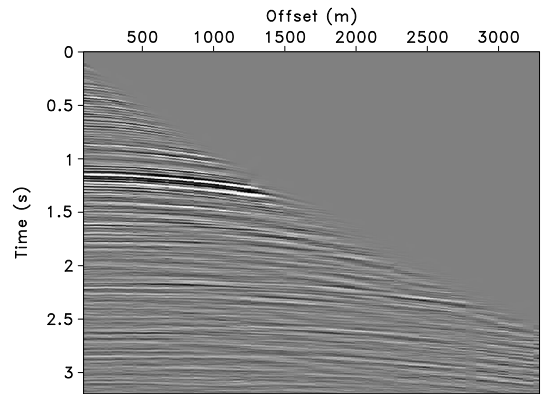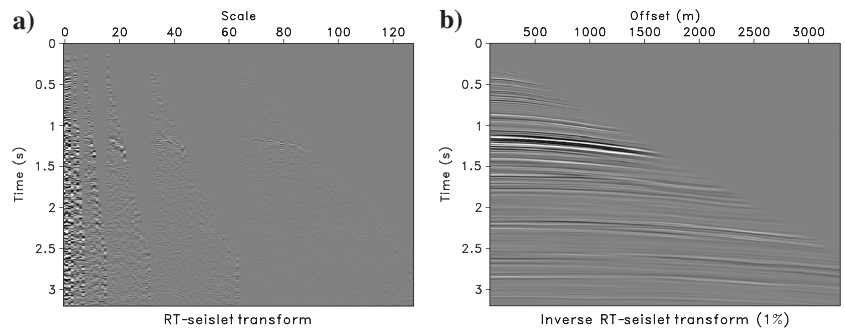

Figure 15. Common-midpoint gather.

Figure 16. (a) The field data in the RT-seislet transform domain and (b) reconstruction using only 1% of significant coefficients by the inverse RT-seislet transform.
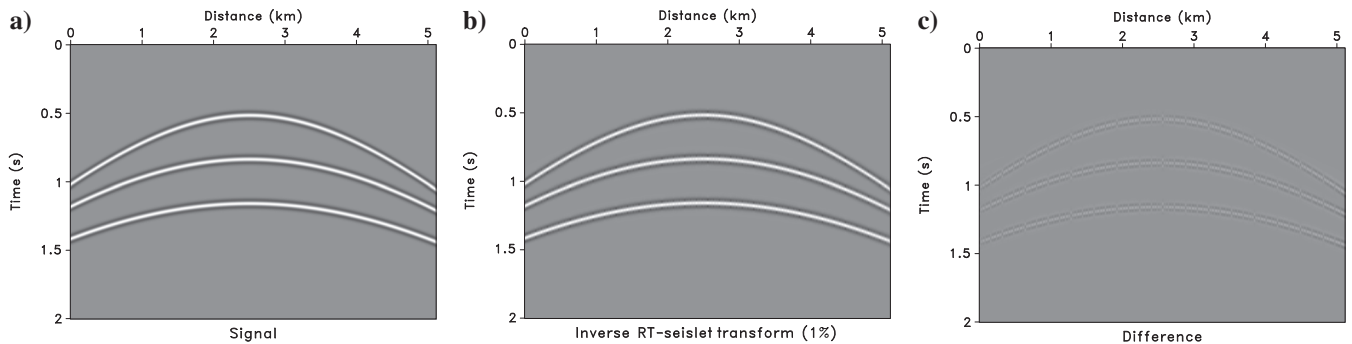

Figure 14. (a) Synthetic shot gather. (b) Data reconstruction by the inverse RT-seislet transform using only 1% of the most significant coefficients. (c) Difference between (a and b).

easily obtained from the predictive painting with multiple reference traces. With the RT volume, the 3D seislet transform can be constructed by cascading the 2D seislet transform along inline and crossline directions. To be specific, we first apply the 2D RT-seislet transform along the inline direction, and then another 2D transform along the crossline is applied on the coefficients from the previous step to obtain the coefficients in the 3D transform domain. The coefficients of the 2D seislet transform along the inline direction and the 3D seislet transform are shown in Figure 22a and 22b. In the seislet domain, most of the coefficients concentrate in the coarse scales, which show the excellent compression ability of the RT-seislet transform. Figure 22c shows the data reconstruction result using only 5% of the most significant coefficients. The difference between Figure 20a and the reconstructed data, contains mainly noise, is shown in Figure 22d. The proposed method has good performance for reconstruction and preserving the structures of the data set.
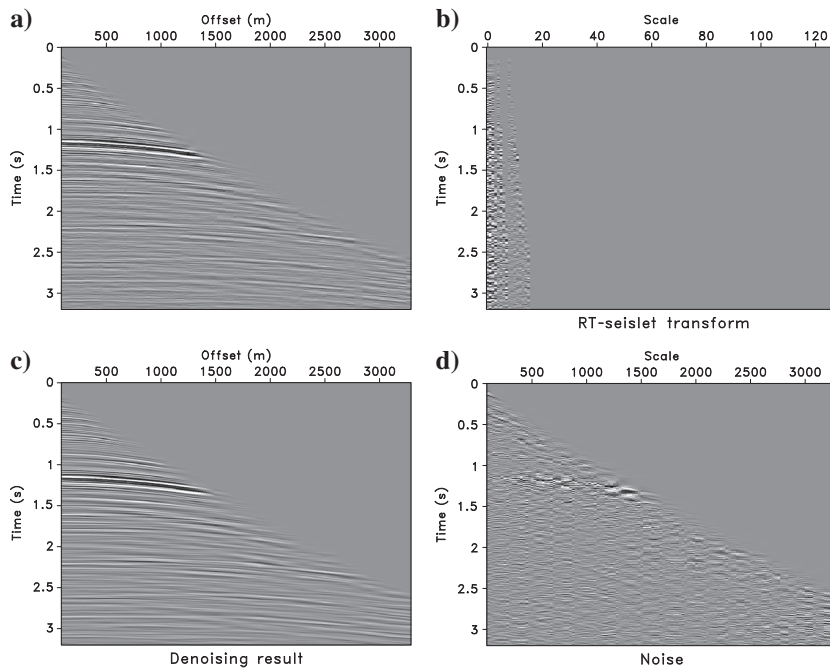

Figure 17. (a) Original gather. (b) Denoised result by muting RT-seislet coefficients at fine scales (a) and (c) the removed noise section using the RT-seislet transform.
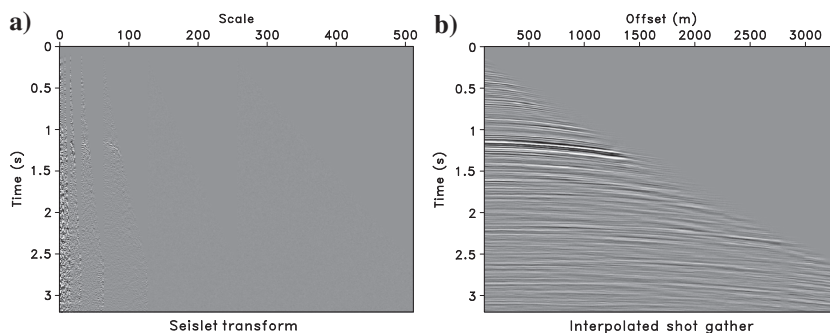

Figure 18. (a) Extended seislet transform domain. (b) Interpolated shot gather by the inverse RT-seislet transform.
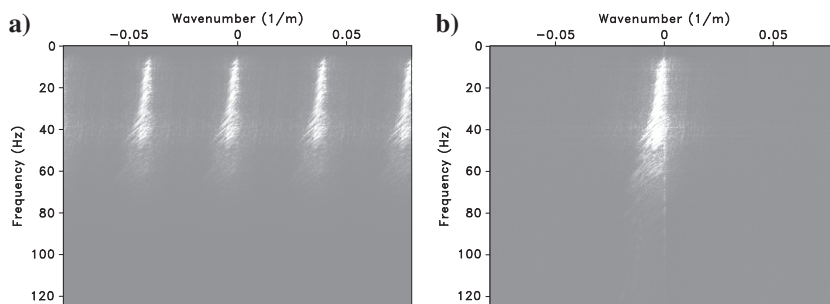

Figure 19. The f-k spectra of the (a) zero-padded and (b) interpolated field data.

DISCUSSION

The proposed formulation of the seislet transform attempts to construct multiscale prediction operators, to enhance the performance of the seislet transform. The prediction operators in the original seislet transform are defined by PWD, so the prediction of distant traces needs recursive computation, which is very time consuming when it comes to a large data set. In the proposed RT-seislet transform, an RT volume is used to define a multiscale prediction operator. As shown in the previous sections, the relationship between any two traces can be obtained from the RT volume, which helps avoid the recursive computation for the prediction of distant traces. As a result, the RT-seislet transform is much more efficient than the original seislet transform.

Besides, in the implementation of the proposed method, the choice of reference traces plays an important role in the generation of the RT volume. More reference traces usually mean a better RT volume. The location of reference traces also needs to be considered carefully. In practice, evenly distributed reference traces are recommended. Besides, complex geologic structures need to be treated differently. For example, it is better to put reference traces at each side of faults. Another important issue is about the smoothing radius when estimating local slopes by PWD. For noise-free data, a small smoothing radius is enough. The smoothing radius is three for the estimation of Figure 2. And with the increasing of the noise level, a larger smoothing radius is needed.

The proposed RT-seislet transform highly depends on the RT volume. In our method, local slopes by PWD, which are easily affected by noise, are used to generate the RT volume, so the new formulation is sensitive to the noise. However, this problem certainly can be solved by improving the PWD or by using other methods, which are not sensitive to noise, to generate the RT volume.
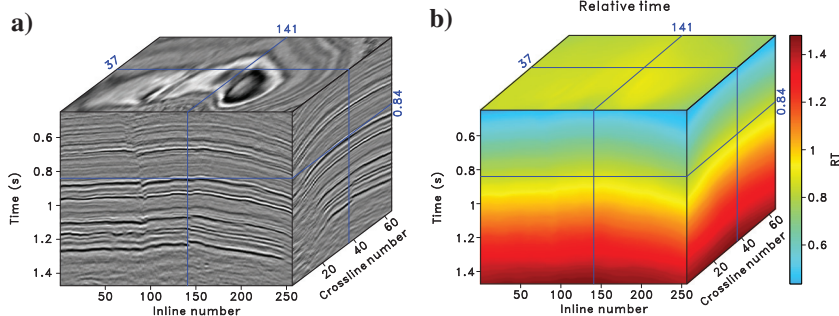
Figure 20. (a) Teapot dome data set and (b) RT volume estimated by the predictive painting.
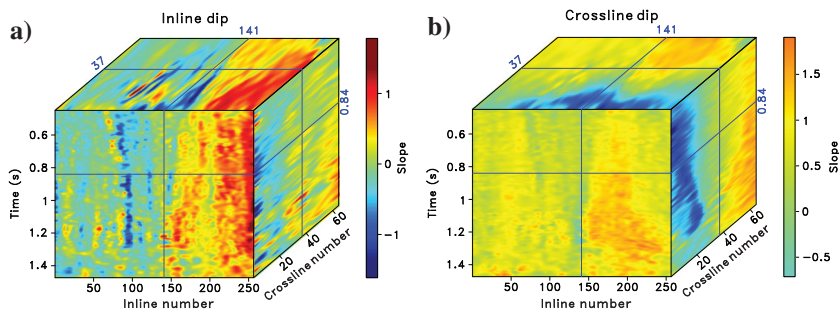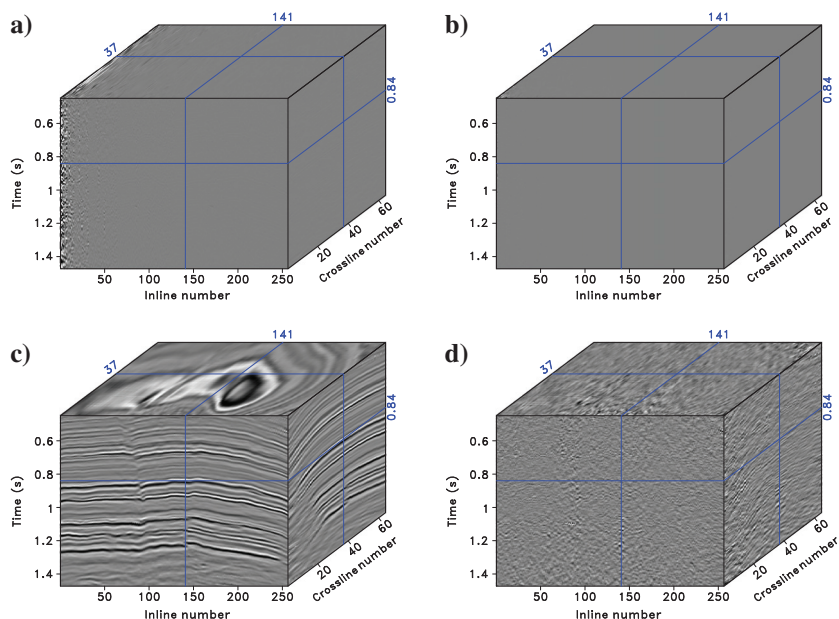

Figure 21. (a) Inline and (b) crossline dip.

Figure 22. (a) The coefficients in the 2D seislet domain along inline only. (b) The coefficients in 3D seislet domain. (c) Data reconstruction using only 5% of significant coefficients by the inverse RT-seislet transform. (d) Difference between (c) and the original seismic volume (Figure 20a).

CONCLUSION

We have proposed a new formulation of the seislet transform, a novel approach to sparse seismic data. In our approach, we use an RT volume to construct multiscale prediction and update operators

for the seislet transform. This proposed approach is computationally more efficient and better preserves geologically meaningful discontinuities than the original formulation of the seislet transform in reconstructing the raw seismic data. It also has excellent performance in obtaining the sparse representation of seismic data. Synthetic and field data examples show that the proposed new formulation is efficient and effective in data reconstruction and noise attenuation.

DATA AND MATERIALS AVAILABILITY

Data associated with this research are available and can be obtained by contacting the corresponding author.

REFERENCES

Bader, S., K. Spikes, and S. Fomel, 2018, Missing well-log data prediction using Bayesian approach in the relative-geologic time domain: 88th Annual International Meeting, SEG, Expanded Abstracts, 804–808, doi: 10.1190/segam2018-2997278.1.
Burnett, W., and S. Fomel, 2009, Moveout analysis by time warping: 79th Annual International Meeting, SEG, Expanded Abstracts, 3710–3714, doi: 10.1190/1.3255639.
Chen, Y., 2016, Dip-separated structural filtering using seislet transform and adaptive empirical mode decomposition based dip filter: Geophysical Journal International, 206, 457–469.
Chen, Y., and S. Fomel, 2018, EMD-seislet transform: Geophysics, 83, no. 1, A27–A32, doi: 10.1190/geo2017-0554.1.
Chen, Y., S. Fomel, and J. Hu, 2014, Iterative deblending of simultaneous-source seismic data using seislet-domain shaping regularization: Geophysics, 79, no. 5, V179–V189, doi: 10.1190/geo2013-0449.1.
Chen, Y., J. Ma, and S. Fomel, 2016, Double-sparsity dictionary for seismic noise attenuation: Geophysics, 81, no. 2, V103–V116, doi: 10.1190/geo2014-0525.1.
Claerbout, J. F., 2000, Basic earth imaging: Stanford Exploration Project, http://sepwww.stanford.edu/sep/prof/bei/toc_html, 28 November 2019.
Cohen, A., I. Daubechies, and J. C. Feauveau, 1992, Biorthogonal bases of compactly supported wavelets: Communications on Pure and Applied Mathematics, 45, 485–560, doi: 10.1002/cpa.3160450502.
Do, M. N., and M. Vetterli, 2005, The contourlet transform: An efficient directional multiresolution image representation: IEEE Transactions on Image Processing, 14, 2091–2106, doi: 10.1109/TIP.2005.859376.
Fomel, S., 2002, Applications of plane-wave destruction filters: Geophysics, 67, 1946–1960, doi: 10.1190/1.1527095.
Fomel, S., 2010, Predictive painting of 3D seismic volumes: Geophysics, 75, no. 4, A25–A30, doi: 10.1190/1.3453847.
Fomel, S., and Y. Liu, 2010, Seislet transform and seislet frame: Geophysics, 75, no. 3, V25–V38, doi: 10.1190/1.3380591.

Fomel, S., P. Sava, I. Vlad, Y. Liu, and V. Bashkardin, 2013, Madagascar: Open-source software project for multidimensional data analysis and reproducible computational experiments: Journal of Open Research Software, **1**, e8, doi: 10.5334/jors.ag.

Gan, S., S. Wang, Y. Chen, and X. Chen, 2016, Simultaneous-source separation using iterative seislet-frame thresholding: IEEE Geoscience and Remote Sensing Letters, **13**, 197–201, doi: 10.1109/LGRS.2015.2505319.

Gan, S., S. Wang, Y. Chen, X. Chen, W. Huang, and H. Chen, 2016, Compressive sensing for seismic data reconstruction via fast projection onto convex sets based on seislet transform: Journal of Applied Geophysics, **130**, 194–208, doi: 10.1016/j.jappgeo.2016.03.033.

Gan, S., S. Wang, Y. Chen, Y. Zhang, and Z. Jin, 2015, Dealiased seismic data interpolation using seislet transform with low-frequency constraint: IEEE Geoscience and Remote Sensing Letters, **12**, 2150–2154, doi: 10.1109/LGRS.2015.2453119.

Hennenfent, G., and F. J. Herrmann, 2006, Seismic denoising with nonuniformly sampled curvelets: Computing in Science Engineering, **8**, 16–25, doi: 10.1109/MCSE.2006.49.

Labate, D., W.-Q. Lim, G. Kutyniok, and G. Weiss, 2005, Sparse multidimensional representation using shearlets: Proceedings of SPIE, **5914**, 59140U, doi: 10.1117/12.613494.

Le Pennec, E., and S. Mallat, 2005, Sparse geometric image representations with bandelets: IEEE Transactions on Image Processing, **14**, 423–438, doi: 10.1109/TIP.2005.843753.

Li, Q., and J. Gao, 2013, Contourlet based seismic reflection data non-local noise suppression: Journal of Applied Geophysics, **95**, 16–22, doi: 10.1016/j.jappgeo.2013.05.002.

Liu, C., P. Li, Y. Liu, D. Wang, X. Feng, and D. Liu, 2013, Iterative data interpolation beyond aliasing using seislet transform: Chinese Journal of Geophysics, **56**, 1619–1627, doi: 10.6038/cjg20130519.

Liu, Y., and S. Fomel, 2010, OC-seislet: Seislet transform construction with differential offset continuation: Geophysics, **75**, no. 6, WB235–WB245, doi: 10.1190/1.3479554.

Liu, Y., S. Fomel, and C. Liu, 2015, Signal and noise separation in prestack seismic data using velocity-dependent seislet transform: Geophysics, **80**, no. 6, WD117–WD128, doi: 10.1190/geo2014-0234.1.

Ma, J., and G. Plonka, 2010, The curvelet transform: IEEE Signal Processing Magazine, **27**, 118–133, doi: 10.1109/MSP.2009.935453.

Starck, J. L., E. J. Candes, and D. L. Donoho, 2002, The curvelet transform for image denoising: IEEE Transactions on Image Processing, **11**, 670–684, doi: 10.1109/TIP.2002.1014998.

Stark, T. J., 2003, Unwrapping instantaneous phase to generate a relative geologic time volume: 73rd Annual International Meeting, SEG, Expanded Abstracts, 1707–1710, doi: 10.1190/1.1844072.

Stark, T. J., 2004, Relative geologic time (age) volumes — Relating every seismic sample to a geologically reasonable horizon: The Leading Edge, **23**, 928–932, doi: 10.1190/1.1803505.

Sweldens, W., 1995, The lifting scheme: A new philosophy in biorthogonal wavelet constructions: Wavelet Applications in Signal and Image Processing III, 68–79, doi: 10.1117/12.217619.

Velisavljevic, V., B. Beferull-Lozano, M. Vetterli, and P. L. Dragotti, 2006, Directionlets: Anisotropic multidirectional representation with separable filtering: IEEE Transactions on Image Processing, **15**, 1916–1933, doi: 10.1109/TIP.2006.877076.

Wu, X., and D. Hale, 2015, Horizon volumes with interpreted constraints: Geophysics, **80**, no. 2, IM21–IM33, doi: 10.1190/geo2014-0212.1.

Wu, X., and G. Zhong, 2012, Generating a relative geologic time volume by 3D graph-cut phase unwrapping method with horizon and unconformity constraints: Geophysics, **77**, no. 4, O21–O34, doi: 10.1190/geo2011-0351.1.